Determination of Proton Transfer Rates by Chemical Rescue: Application to Bacterial Reaction Centers†

M. L. Paddock,‡ P. Ädelroth,‡,§ G. Feher,‡ M. Y. Okamura,*,‡ and J. T. Beatty‖

Department of Physics 0319, University of California—San Diego, 9500 Gilman Drive, La Jolla, California 92093-0319, and Department of Microbiology and Immunology, University of British Columbia, Vancouver, BC V6T 1Z3, Canada

Received June 14, 2002; Revised Manuscript Received October 1, 2002

ABSTRACT: The bacterial reaction center (RC) converts light into chemical energy through the reduction of an internal quinone molecule Q_B to Q_BH_2. In the native RC, proton transfer is coupled to electron transfer and is not rate-controlling. Consequently, proton transfer is not directly observable, and its rate was unknown. In this work, we present a method for making proton transfer rate-controlling, which enabled us to determine its rate. The imidazole groups of the His-H126 and His-H128 proton donors, located at the entrance of the transfer pathways, were removed by site-directed mutagenesis (His → Ala). This resulted in a reduction in the observed proton-coupled electron transfer rate [$(Q_A^{-\bullet}Q_B)Glu^- + H^+ \rightarrow (Q_AQ_B^{-\bullet})GluH$], which became rate-controlled by proton uptake to Glu-L212 [Ädelroth, P., et al. (2001) *Biochemistry 40*, 14538−14546]. The proton uptake rate was enhanced (rescued) in a controlled fashion by the addition of imidazole or other amine-containing acids. From the dependence of the observed rate on acid concentration, an apparent second-order rate constant $k_{(2)}$ for the "rescue" of the rate was determined. $k_{(2)}$ is a function of the proton transfer rate and the binding of the acid. The dependence of $k_{(2)}$ on the acid pK_a (i.e., the proton driving force) was measured over 9 pK_a units, resulting in a Brönsted plot that was characteristic of general acid catalysis. The results were fitted to a model that includes the binding (facilitated by electrostatic attraction) of the cationic acid to the RC surface, proton transfer to an intermediate proton acceptor group, and subsequent proton transfer to Glu-L212. A proton transfer rate constant of $\sim 10^5$ s^{-1} was determined for transfer from the bound imidazole group to Glu-L212 (over a distance of ~20 Å). The same method was used to determine a proton transfer rate constant of 2×10^4 s^{-1} for transfer to $Q_B^{-\bullet}$. The relatively fast proton transfer rates are explained by the presence of an intermediate acceptor group that breaks the process into sequential proton transfer steps over shorter distances. This study illustrates an approach that could be generally applied to obtain information about the individual rates and energies for proton transfer processes, as well as the pK_as of transfer components, in a variety of proton translocating systems.

The field of bioenergetics deals to a large extent with the study of electron and proton transfer reactions catalyzed by membrane proteins. With the determination of the three-dimensional structures of several membrane-bound complexes involved in energy conversion, we are now in a position to address in detail the mechanisms of these processes. Of fundamental importance to the understanding of these reactions is the determination of the rate constants for the individual reaction steps. Because many of these reactions involve proton transfer, the determination of their rate constants is crucial for achieving a basic understanding of these processes. In many cases, proton transfer is coupled to other reactions that are rate-controlling and, consequently, proton transfer cannot be directly assessed.

We report here a general strategy for determining the proton transfer rate constant in such a system. We apply this approach to proton transfer in the bacterial reaction center (RC)[1] from *Rhodobacter* (*Rb.*) *sphaeroides*, which is a transmembrane protein complex that catalyzes the light-induced electron and proton transfer reactions leading to reduction and protonation, respectively, of a bound quinone molecule Q_B (eq 1) (*1*, *2*).

† This work was supported by the National Science Foundation (Grant MCB99-82186), the National Institutes of Health (Grants GM 41637 and NIH GM 13191), the Canadian Institutes of Health Research, and a postdoctoral fellowship from the Swedish Foundation for International Cooperation in Research and Higher Education (STINT) to P.Ä.

* To whom correspondence should be addressed. Phone: (858) 534-2505. Fax: (858) 822-0007. E-mail: mokamura@ucsd.edu.

‡ University of California—San Diego.

§ Current address: Department of Biochemistry and Biophysics, The Arrhenius Laboratories for Natural Sciences, Stockholm University, SE-106 91 Stockholm, Sweden.

‖ University of British Columbia.

[1] Abbreviations: Q_A and Q_B, primary and secondary quinone electron acceptor molecules, respectively; double mutant, HA(H126)/HA(H128) [His-H126 → Ala/His-H128 → Ala] mutant; A^-, intermediate proton acceptor group; R, generic deprotonated rescuing acid molecule; RH^+, rescuing cationic acid molecule; $k_{(2)}$, apparent second-order rate constant; K_D, dissociation constant of the acid; k_{on} and k_{off}, on and off rate constants, respectively, for binding of the acid; k_1 and k_{-1}, forward and reverse rate constants, respectively, for proton transfer from RH^+ to A^-; k_2, forward rate constant for proton transfer from AH to Glu-L212; k_{ET}, overall electron transfer rate constant; k_{H^+}, overall proton transfer rate constant; Q_B, secondary quinone.

10.1021/bi020419x CCC: $22.00
Published on Web 11/20/2002

$$Q_B + 2e^- + 2H^+ + 2h\nu \xrightarrow{RC} Q_BH_2 \qquad (1)$$

Light absorbed by the RC initiates the photoionization of the primary donor, D, a bacteriochlorophyll dimer. Electrons are transferred via a bacteriochlorophyll and bacteriopheophytin to the primary quinone Q_A and then to Q_B, the secondary quinone. In photosynthetic membranes, the protons required for the reduction of the quinone to quinol (eq 1) come from the cytoplasm. The Q_BH_2 leaves the RC and is oxidized by the cytochrome bc_1 complex, from which the quinol protons are released into the periplasm. This creates a proton gradient across the membrane that drives ATP synthesis.

The double reduction of Q_B takes place in two sequential light-induced proton-coupled electron transfer reactions that can be monitored by time-resolved optical absorption spectroscopy (*1*−*5*). In this study, we focus on the first electron transfer from $Q_A^{-\bullet}$ to Q_B, the pseudo-first-order rate constant $k_{AB}^{(1)}$, which can be directly measured through transient absorbance changes (*3*−*6*). A prerequisite for electron transfer is the protonation of Glu-L212 (*3*−*9*). Above pH ~8.5, $k_{AB}^{(1)}$ decreases with increasing pH due to the ionization of Glu-L212 and other coupled carboxylic acid groups (*5*−*10*). We represent this reaction as a two-step process shown in eq 2.

$$(Q_A^-\,Q_B)Glu^- + H^+ \xrightarrow{k_{H^+}} (Q_A^-\,Q_B)GluH \xrightarrow{k_{ET}} (Q_AQ_B^-)GluH \qquad (2)$$

where Glu represents Glu-L212, k_{H^+} is the rate constant for proton transfer from the RC surface to Glu-L212, which is the rate-controlling step in proton uptake from solution, and k_{ET} (10^4−10^5 s^{-1}) (*3*−*5*, *11*−*16*) is the observed rate of electron transfer. In the native RC, uptake of H^+ is fast and reversible; i.e., $k_{H^+} > k_{AB}^{(1)}$. Thus, the kinetics of the $Q_A^{-\bullet}Q_B \rightarrow Q_AQ_B^{-\bullet}$ electron transfer at high pH result in a single exponential with a rate constant equal to k_{ET} times the steady state fraction of protonated Glu-L212, which has been assigned a pK_a value in the range of 8.5−10 (*3*−*6*).[2] The proton from Glu-L212 is subsequently transferred to reduced Q_B, supplying one of the two protons involved in forming Q_BH_2 (*1*, *3*−*5*).

The Q_B molecule is located in the interior of the RC, without direct contact with the cytoplasm (*17*−*20*). The pathway for proton transfer has been shown by site-directed mutagenesis and metal binding studies to involve Asp-L213 (*3*, *21*, *22*), Asp-L210 and Asp-M17 (*8*, *23*), and the surface His-H126 and His-H128 (*24*), which connect the cytoplasmic surface of the protein to Glu-L212 (Figure 1). The nearby Pro-L209 has been proposed to participate in the pathway based on changes in the observed rate of proton uptake upon

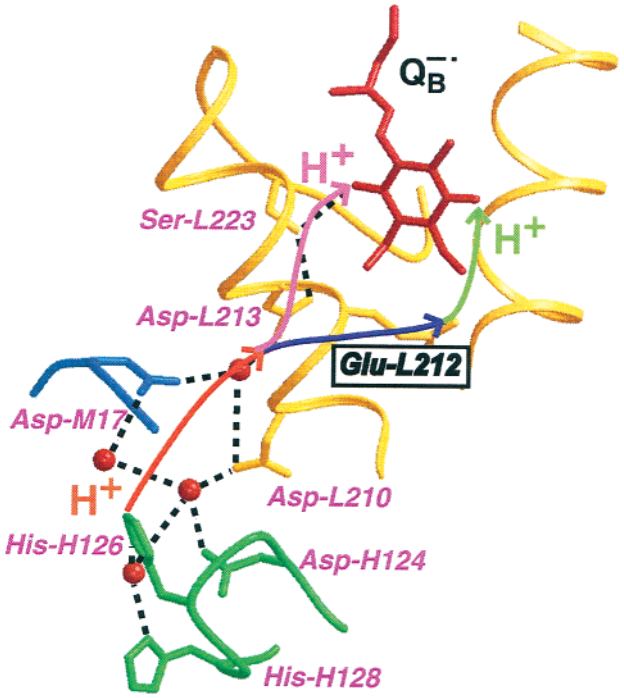

FIGURE 1: Part of the reaction center crystal structure showing the proton transfer pathways in *Rb. sphaeroides*. Water molecules are shown as spheres. Potential hydrogen bonds are represented by dashed lines. The proton transfer pathways connecting the surface to the Q_B site share the entry point and several carboxylic acids (red line) before branching to Glu-L212 (blue line) or to $Q_B^{-\bullet}$ (magenta line). Although protonation (neutralization) of Glu-L212 is required for the first electron reduction of Q_B to proceed (eq 2), this proton is transferred to the proximal oxygen of reduced Q_B only after formation of Q_BH^- (green line) (*2*). The coordinates were obtained from PDB entry 1AIJ (*18*).

its replacement (*20*). However, since Pro is not a protonatable residue, we believe that its effect is brought about by structural changes. Even though the proton pathway is quite long (~20 Å), the rate of proton uptake in the native RC is not rate-controlling and, hence, k_{H^+} is not directly measurable. This raises the following questions: (i) how fast is proton transfer, and (ii) how is the relatively fast transfer achieved?

To address these questions, we developed a system in which proton transfer was rate-controlling by removing key functional groups. The two surface His residues at positions 126 and 128 were replaced with Ala [HA(H126)/HA(H128)], thereby removing the imidazole groups (*24*). In this double-mutant RC, the proton transfer k_{H^+} became the rate-controlling step for $k_{AB}^{(1)}$ (eq 2). Measurements of $Q_B^{-\bullet}$ stability and proton uptake were like in the native RC, suggesting little if any structural or electrostatic alteration at the Q_B site resulting from the amino acid replacements (*24*). Fast proton transfer could be restored (rescued) by adding chemical analogues of the removed group, as has been previously performed in other systems (*26*−*31*).

When pH > pK_a(Glu-L212), the observed rate constant $k_{AB}^{(1)}$ in this double-mutant RC was increased by the addition of cationic proton donors such as imidazole (*24*). At low concentrations, the increase was directly proportional to the concentration of protonated imidazole ([ImidH$^+$]) as expressed in eq 3:

$$k_{H^+} = k_{AB}^{(1)} = k_{BCKGD} + k_{(2)}[ImidH^+] \qquad (3)$$

[2] The assignment of the apparent pK_a to a single group is an approximation, since there are many titrating groups in the RC that interact electrostatically, leading to nonclassic titration behavior (*7*−*10*). However, experimental results have shown that at pH 9, at which our measurements were taken, Glu-L212 is the major contributor (*3*−*6*).

where k_{BCKGD} is the background rate constant observed with no added acid, attributed to proton delivery by H_3O^+ (*24*), and $k_{(2)}$ is an apparent second-order rate constant that contains information about the rate of proton transfer to Glu-L212. A correlation between $k_{(2)}$ and the pK_a of the rescuing acid was observed (*32*) which provides additional support for the structural and electrostatic near equivalence of the native and double-mutant RCs. If the effect of the mutation were due to secondary effects such as a structural or electrostatic change, a correlation between $k_{(2)}$ and pK_a would not be expected.

Having established that this system is a good analogue for the native RC, we proceed in this paper to analyze the observed behavior to obtain information about the individual molecular steps involved in the proton transfer process. Our strategy was to investigate the rate of proton transfer as a function of the driving force for proton transfer (ΔG_H) by using rescuing acids, RH^+, with different pK_a values that result in changes in $k_{(2)}$. Modeling of the observed dependence of $k_{(2)}$ on ΔG_H required the introduction of an intermediate acceptor state and enabled us to determine the proton transfer rate constant k_{H^+} and the energy profile for the proton transfer process.

MATERIALS AND METHODS

Reagents and Quinones. Q_{10} (2,3-dimethoxy-5-methyl-6-decaisoprenyl-1,4-benzoquinone) was obtained from Sigma, prepared in ethanol, dried under nitrogen, and solubilized in 1% LDAO (lauryl dimethylamine *N*-oxide). The following acids were used in this study: pyrimidine ($pK_a = 1.2$), triazole ($pK_a = 2.3$), 4(5)-imidazolecarboxaldehyde ($pK_a \sim 4$), 1-methylimidazole ($pK_a = 7.0$), imidazole ($pK_a = 7.0$), and morpholine ($pK_a = 8.4$), obtained from Aldrich; pyridine ($pK_a = 5.4$), 2-methylimidazole ($pK_a = 8.0$), and piperazine ($pK_a = 9.7$) from Fluka; trimethylamine ($pK_a = 9.8$) and methylamine ($pK_a = 10.5$) from Sigma; tris ($pK_a = 8.3$) from Boehringer Mannheim; and ammonia ($pK_a = 9.0$) from Fisher. All other reagents were of analytical grade.

Site-Directed Mutagenesis and Preparation of Reaction Centers. The His-H126 → Ala/His-H128 → Ala [HA(H126)/HA(H128)] double mutant was constructed as described previously (*24*, *33*). RCs from *Rb. sphaeroides* R26.1 and mutant strains were purified to an A^{280}/A^{800} ratio of ≤1.3 in LDAO as described previously (*34*). The Q_B site was reconstituted by addition of a 3−4-fold excess of Q_{10} in 1% LDAO, followed by dialysis against 15 mM Tris, 0.1 mM EDTA, and 0.04% β-D-dodecyl maltoside.

Electron Transfer Measurements. Absorbance changes in response to a laser flash were measured using a setup of local design (*12*). Actinic illumination was provided by a Nd:YAG laser (Opotek, Carlsbad, CA). The pseudo-first-order rate constant $k_{AB}^{(1)}$ for electron transfer (eq 2) was determined from transient absorbance changes monitored at 750 nm following a single laser flash. The spectral changes result from a charge-induced spectral shift of a nearby bacteriopheophytin molecule (*11*−*16*). The observed kinetics were fitted to the sum of two exponentials. The rate constant for the major phase (~75% at pH 9) is associated with proton uptake and is attributed to the fraction of RCs with Glu-L212 initially ionized (*24*);[3] this fraction is determined by the difference between the pK_a of ~8.5 and the operating pH of 9. The observed rate, which depends on the acid concentration, is the focus of this work. The minor phase (~25%) was not associated with proton uptake and had the same rate constant as in the native RC. The conditions were 2 μM RCs in 50 mM KCl, 0.04% β-D-dodecyl maltoside, pH 9, and 21 °C.

Fittings. All fittings were performed using the nonlinear fitting algorithm Origin 6.1 (OriginLab Corp.).

Model for the Dependence of $k_{AB}^{(1)}$ on Acid Concentration. The dependence of $k_{AB}^{(1)}$ in the double-mutant RC on acid concentration (eq 4) was modeled with the Michaelis−Menten equation (eq 4).

$$k_{AB}^{(1)} - k_{BCKGD} = \frac{k_{cat}[RH^+]}{[RH^+] + K_M} \quad (4)$$

where $[RH^+]$ is the concentration of the cationic rescuing acid, k_{cat} is the catalytic or limiting rate constant, and K_M is the Michaelis−Menten constant, which is equal to $k_{cat}/k_{(2)}$ (*35*). The concentration of acid was calculated from the total concentration of the rescuer $[R]_{total}$ and its solution pK_a $[[RH^+] = [R]_{total}/(1 + 10^{pH-pK_a})]$. At a low RH^+ concentration, eq 4 simplifies to $k_{AB}^{(1)} - k_{BCKGD} = k_{(2)}[RH^+]$ (eq 3). Thus, the apparent second-order rate constant $k_{(2)}$ can be determined from the initial slope of a plot of $k_{AB}^{(1)}$ versus $[RH^+]$. At high acid concentrations, the rate reaches a limiting value given by k_{cat}. For all of the measurements reported in this work, $k_{cat} = k_{H^+}k_{ET}/(k_{H^+} + k_{ET})$ (*35*). Under conditions in which internal proton transfer remains rate-controlling ($k_{ET} > k_{H^+}$) at all acid concentrations, $k_{cat} = k_{H^+}$ and $K_M = K_D$ (*35*), the dissociation constant of the acid.

RESULTS

In this study, we measured the effect of adding exogenous acids on the rate of proton delivery from the surface of the RC to internal proton acceptor groups in the HA(H126)/HA(H128) mutant RC (hereafter called the double mutant), which lacks the surface imidazole groups of the native His at the entrance of the proton transfer pathways (*24*). It had been shown previously that the measured rate of proton uptake from solution is the same as the coupled rate of electron transfer to Q_B (eq 2) in the double mutant RC (*24*). This result is explained by the strong proton−electron coupling and the required protonation of Glu-L212 (eq 2). Thus, the electron transfer rate provides a measure of the rate of proton transfer to Glu-L212 in the double-mutant RC.

Dependence of $k_{AB}^{(1)}$ on Acid Concentration: Determination of the Second-Order Rate Constant $k_{(2)}$ and the Dissociation Constant K_D of the Acid. An important aspect of the rescue process in the double mutant is the interaction between the acid and the RC surface. This process was investigated by measuring the dependence of the first electron transfer (eq 2) on acid concentration. We measured this dependence at pH 9, where the maximal difference between the double mutant and native rates was observed (*24*). In the double mutant, the observed kinetics exhibited two phases (Figure 2). The major phase (~75%) is associated with

[3] For simplicity, we assign the measured kinetic pK_a of 8.5 to Glu-L212. The coupling to other carboxylic acid groups leads to a small (and difficult to determine) correction to this value (see footnote 2).

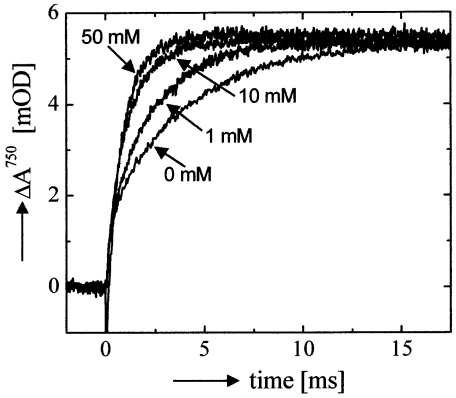

FIGURE 2: Proton-coupled electron transfer rate of eq 2 [$(Q_A^{-\bullet}Q_B)Glu^- + H^+ \rightarrow (Q_AQ_B^{-\bullet})GluH$] in the double mutant RC for the indicated imidazole concentrations. The kinetic rise has two phases. The smaller, faster phase is attributed to the fraction of RCs in which Glu-L212 is initially protonated at pH 9 ($pK_a \cong 8.5$) (*24*). The larger, slower phase is attributed to the fraction of the RCs in which Glu-L212 is initially ionized. The slower phase is a consequence of slow proton delivery to the RC surface (*24*). This phase was fitted to a single exponential (not shown) with a rate constant $k_{AB}^{(1)}$. As the concentration of imidazole was increased, $k_{AB}^{(1)}$ increased, but the amplitude remained constant. At 50 mM imidazole, $k_{AB}^{(1)}$ was essentially the same as measured in the native RC. Experimental conditions: 2 μM RC, 50 mM KCl, 0.04% β-D-dodecyl maltoside, pH 9, and 21 °C (average of ~15 traces).

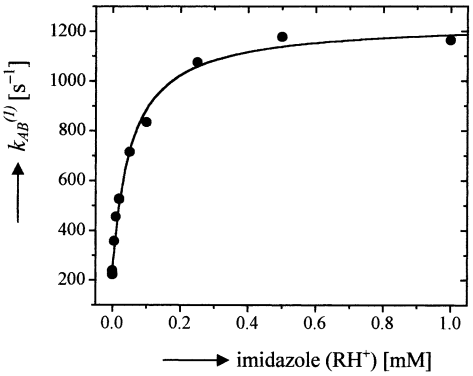

FIGURE 3: Dependence of the slow phase of $k_{AB}^{(1)}$ on the concentration of protonated imidazole (RH^+). The value of $k_{AB}^{(1)}$ was determined from an exponential fit to the slow phase of the kinetic rise (see Figure 2). In the double mutant, $k_{AB}^{(1)}$ is limited by the rate of proton delivery to the RC surface (*24*), which depends on the concentration of the proton-carrying imidazole. The second-order rate constant $k_{(2)}$ was obtained from a fit of eq 4 to the data (solid line). At high imidazole concentrations, $k_{AB}^{(1)}$ reaches the native value, which becomes rate-controlled by electron transfer k_{ET} (eq 2). The conditions were the same as those described in the legend of Figure 2.

proton uptake from solution and is attributed to rate-controlling proton uptake to Glu-L212 in the major fraction of RCs with Glu-L212 initially ionized; under these conditions, Glu-L212 has an apparent pK_a of ~8.5 (*24*).[3] This slow phase was ~6-fold slower than in the native RC, but its rate could be increased (rescued) by the addition of imidazole ($pK_a \sim 7.0$) to native-like values (1200 s^{-1}) (Figure 3) which become rate-controlled by electron transfer (*24*). We will focus on this phase and call it $k_{AB}^{(1)}$ throughout the remainder of this paper. The minor phase (~25%) occurs in the fraction of RCs that contain protonated Glu-L212 and is not associated with proton uptake (*24*); this phase has the same rate constant as the native RC. The dependence of $k_{AB}^{(1)}$ on the acid concentration was determined (Figure 3) and eq 4 used

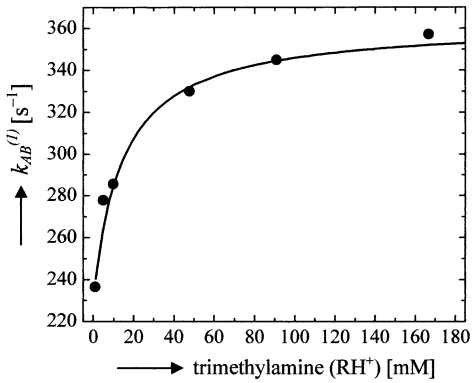

FIGURE 4: Dependence of the slow phase of $k_{AB}^{(1)}$ on the concentration of protonated trimethylamine (RH^+). Since the rescued value of $k_{AB}^{(1)}$ is smaller than the native value (see Figure 3), the observed rate remains limited by the rate of proton delivery. Thus, from the fit to eq 4 (solid line), we obtain a dissociation constant K_D of 10 ± 2 mM. The conditions were the same as those described in the legend of Figure 2.

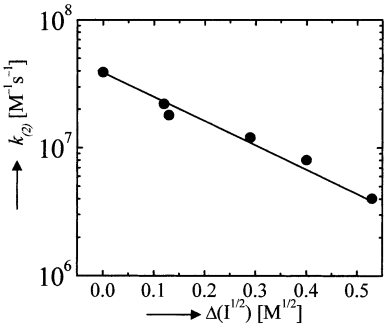

FIGURE 5: Second-order rate constant $k_{(2)}$ for imidazole as a function of the change in the square root of the ionic strength $\Delta(I)^{1/2}$, with reference to $I = 10$ mM. The decrease in $k_{(2)}$ with increasing $I^{1/2}$ shows that electrostatic attraction enhances proton delivery to the RC surface. This shows that the protonated cationic form of the acid is the active form. The solid line is a least-squares fit of the data to eq 11. The slope is −1.9 ± 0.1. The conditions were the same as those described in the legend of Figure 2.

to obtain $k_{(2)}$. For imidazole ($C_3N_2H_5^+$, $pK_a = 7.0$), $k_{(2)}$ equaled (2.2 ± 0.2) × 10^7 M^{-1} s^{-1} at pH 9.0. This rate exhibited a weak pH dependence, decreasing ~2-fold as the pH was increased from pH 8.5 to 9.5.

For trimethylammonium [$(CH_3)_3NH^+$, $pK_a = 9.8$], $k_{AB}^{(1)}$ reached a limiting value of 360 s^{-1} (Figure 4), which is 130 s^{-1} greater than the background rate. Since this rate constant is significantly smaller than k_{ET}, proton transfer remained rate-controlling at all acid concentrations. Therefore, K_M in eq 4 is the dissociation constant K_D of the acid molecule ($K_D \cong 10 \pm 2$ mM; see legend of Figure 4).

Dependence of $k_{(2)}$ on Salt Concentration. To assess the importance of electrostatic interaction between the acid and the RC surface, the salt dependence of the measured second-order rate constant $k_{(2)}$ for imidazole was determined (eq 4). The value of $k_{(2)}$ decreased as the salt (KCl) concentration increased. For imidazole as the rescuing acid, log $k_{(2)}$ decreased linearly as a function of the change in the square root of the ionic strength, $\Delta(I^{1/2})$, with a slope of −1.9 ± 0.1 (Figure 5).

Dependence of $k_{(2)}$ on Acid pK_a: Brönsted Plot. In addition to imidazole, other small cationic acids could "rescue" $k_{AB}^{(1)}$ in the double mutant RC. The second-order rate constant $k_{(2)}$ was determined at pH 9.0 for each rescuing acid, and

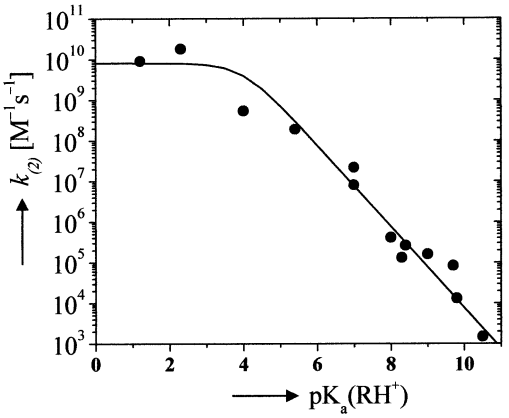

FIGURE 6: Brönsted plot of $k_{(2)}$ as a function of the pK_a of the rescuing acid in the double mutant RC. The values of $k_{(2)}$ were obtained from the fit of eq 4 to the observed dependence of $k_{AB}^{(1)}$ on the acid concentration (see Figures 2 and 3). Below a pK_a of ~4, $k_{(2)}$ reaches the diffusion limit of $\sim 10^{10}$ M^{-1} s^{-1}. At higher pK_a values, $k_{(2)}$ decreases with increasing pK_a, characteristic of general acid catalysis (*36*). The slope of $k_{(2)}$ vs pK_a changes when the pK_a of the bound donating acid matches that of the acceptor. Since the pK_a of the final acceptor Glu-L212 is much larger ($pK_a \sim 8.5$) than the pK_a of the rescuing cationic acid at the break of the Brönsted plot, an intermediate acceptor group must exist (A^-) within the proton transfer pathway. The data were fitted (solid line) using a steady state approximation (eq 7) and the pK_a dependence of eq 8 (Table 1). Note the good quality of the fit over the range of ~9 pK_a units. The donors that were used were (from lower to higher pK_a) pyrimidine ($pK_a = 1.2$), triazole ($pK_a = 2.3$), 4(5)-imidazolecarboxaldehyde ($pK_a \sim 4$), pyridine ($pK_a = 5.4$), imidazole ($pK_a = 7.0$), 1-methylimidazole ($pK_a = 7.0$), 2-methylimidazole ($pK_a = 8.0$), tris ($pK_a = 8.3$), morpholine ($pK_a = 8.4$), ammonia ($pK_a = 9.0$), piperazine ($pK_a = 9.7$), trimethylamine ($pK_a = 9.8$), and methylamine ($pK_a = 10.5$). The conditions were the same as those described in the legend of Figure 2.

the value of $k_{(2)}$ as a function of the pK_a of the acid (Brönsted plot) (*36*) is plotted in Figure 6. The maximum value of $\sim 10^{10}$ M^{-1} s^{-1} was observed for acids with a pK_a below 4 (Figure 6). For acids with a pK_a above 4, $k_{(2)}$ decreased with increasing pK_a with a Brönsted coefficient α (the negative slope of the line) of 1.0 ± 0.1. To generate the Brönsted plot, cationic acids with pK_a values ranging from 1.2 to 10.5 were used (see Materials and Methods).

Cationic acids with pK_a values of >11 did not result in a measurable enhancement of the observed rate, nor did neutral [dimethylarsinic acid, $(CH_3)_2AsO_2H$, $pK_a \sim 7.5$] or anionic [bicarbonate, HCO_3^-, $pK_a \sim 10$] acids up to a concentration of 0.5 M. In addition, cationic nonprotonatable analogues, such as tetramethylammonium [$(CH_3)_4N^+$], did not enhance the observed rate.

DISCUSSION

The main goal of this work was to determine the proton transfer rate constant k_{H^+} for transfer from the surface of the RC to Glu-L212, the final acceptor in the first proton-coupled electron transfer reaction (eq 2). The underlying difficulty in obtaining information about proton transfer processes in the native RC is that proton transfer is not rate-controlling and therefore cannot be directly observed. To overcome this difficulty, we used the double mutant RC [His-H126 → Ala/His-H128 → Ala]. This mutant lacks the surface imidazole groups at the entrance of the proton transfer pathways, which results in proton transfer becoming rate-controlling (*24*). Addition of various acids resulted in increases in k_{H^+}, which were reflected in larger values of $k_{AB}^{(1)}$ (eq 2) that were related to the concentration and pK_a of the acid. From the dependence of the observed rate on the acid concentration, we obtained an apparent second-order rate constant $k_{(2)}$, which is a function of the individual rate constants for proton transfer in this multicomponent pathway (Figure 1). Crucial to the understanding of the proton transfer processes is the determination of $k_{(2)}$ over an extensive range of acid pK_a values (>9 pK_a units) and the development of a kinetic model to describe the observed behavior. Since previous kinetic results suggest that the Q_B site of this mutant RC is structurally and electrostatically analogous to that of the native RC (*24*), the results obtained on the mutant RC should be applicable to the native system. We begin our discussion with a qualitative description of the observed pK_a dependence of $k_{(2)}$.

General Acid Catalysis: Evidence for an Intermediate Proton Acceptor Group. The observed dependence of $k_{(2)}$ on the pK_a of the acid (Brönsted plot, Figure 6) is characteristic of general acid catalysis (*37*). Figure 6 shows that for low-pK_a acids [$pK_a(RH^+) < 4$], $k_{(2)}$ reaches the diffusion limit for small molecules of $\sim 10^{10}$ M^{-1} s^{-1}. This indicates that the reaction is rate-controlled by the diffusion of the rescuing acid, the ultimate limitation for bimolecular reactions. For higher-pK_a acids [$pK_a(RH^+) > 4$], $k_{(2)}$ decreases with increasing pK_a. The negative slope of log $k_{(2)}$ with pK_a is the Brönsted coefficient α. In our case, $\alpha \cong 1$. In general, one seldom observes an α close to unity, because the observed rate is usually dominated by the strongest acid in solution, i.e., H_3O^+ ($pK_a = -1.7$). However, at pH 9 at which our experiments were performed (because of the largest difference between the double-mutant rate and the native rate), the concentration of H_3O^+ is very small (1 nM), resulting in a background rate k_{BCKGD} (eq 3) that is ~6-fold smaller than the native value for $k_{AB}^{(1)}$.

The change in the slope of the Brönsted plot occurs at a pK_a at which the rate-controlling step of $k_{(2)}$ changes. This happens when the pK_a of the donating acid[4] approximately matches that of the acceptor group, which in our data occurs near a pK_a of 4 (Figure 6).[5] At this pH, there is a change from a proton transfer-controlled rate (for higher-pK_a acids)

[4] We use the pK_a value that corresponds to the pH at which half of the acid is protonated. The pK_a of an individual site of a diprotic acid in which the two protonation sites are equivalent, such as imidazole, is larger by 0.3 unit than the pH at which half of the acid is protonated (*40*). Thus, the extent of proton equilibration to A^- is *decreased* 2-fold. However, the level of binding of the acid to the RC surface is *increased* (up to 2-fold) due to the equivalence of the two protonation sites (as seen later in the Results). Because these two effects are compensatory, the overall effectiveness of the acid is approximately reflected in the designated pK_a values. This statement is supported by the equivalent values of $k_{(2)}$ measured for a monoprotic acid (1-methylimidazole) and a diprotic acid (imidazole) with the same pK_a as defined above.

[5] For the situation of proton transfer between two molecules (RH^+ and A^-) in solution, the change in the slope of the Brönsted plot occurs when $pK_a(RH^+) = pK_a(AH)$ (*37*). In our case, where an intermediate state exists, the onset of the pK_a dependence occurs only approximately when $pK_a(RH^+) \cong pK_a(AH)$. Strictly speaking, the onset occurs when $k_{off} \cong k_{H^+}$, where $k_{H^+} = k_1k_2/(k_{-1} + k_2)$ (eq 13). Since $k_2 > k_{-1}$ (Table 1), the change in slope occurs when $k_{off} \cong k_2k_1/k_{-1} = k_2\{10^{-[pK_a(RH^+) - pK_a(AH)]}\}$, which can be rewritten as $pK_a(RH^+) = pK_a(AH) + \log(k_2/k_{off})$. $\text{Log}(k_2/k_{off})$ has a value of ~2 (Table 1), which results in the onset of the pK_a dependence of $k_{(2)}$ when $pK_a \cong 4$ (Figure 6), being ~2 pK_a units greater than $pK_a(AH)$.

to a diffusion-controlled rate (for lower-pK_a acids). Because the final acceptor group (Glu-L212) is known to have a much higher pK_a of ~8.5 (*3*−*5*), the group responsible for the change in the slope of the Brönsted plot must be an intermediate acceptor group in the proton transfer pathway. This protonated group has become energetically more stable than the protonated acids (RH^+) having a pK_a of <4. It should be noted that the intermediate state would not have been detected without the use of acids with pK_a values that are much smaller (by ≥5 units) than that of imidazole, the chemical equivalent of the removed side chains.

With the inclusion of this postulated intermediate proton acceptor group that we shall call A^-, the rescue of $k_{AB}^{(1)}$ is composed of five steps. Four of these steps [(1) the binding of the rescuing acid, RH^+, (2) proton transfer to an intermediate proton acceptor group, A^-, (3) proton transfer to the final proton acceptor group, Glu^-, and (4) dissociation of the neutral acid, R] lead to the protonation of Glu-L212 (eq 5a).

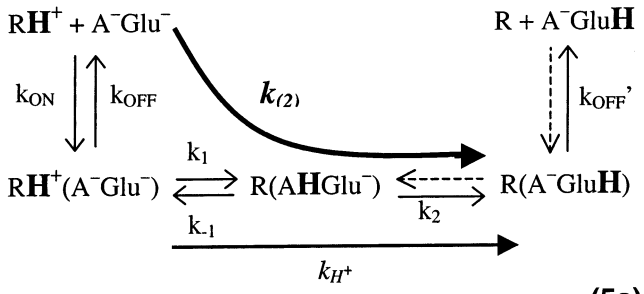

(5a)

where RH^+ and R are the protonated and unprotonated forms of the acid, respectively, A^- is the intermediate proton acceptor group, Glu is the final proton acceptor Glu-L212 (eq 2), k_{on} and k_{off} are the on and off rate constants of the acid molecule, respectively, k_{off}' is the off rate of the unprotonated acid molecule, k_1 and k_{-1} are the forward and reverse proton transfer rate constants for transfer from the acid to A^-, respectively, and k_2 is the forward proton transfer rate constant for transfer from AH to Glu-L212.

The fifth step (eq 5b) is the subsequent electron transfer to Q_B.

$$(Q_A^{-\bullet}Q_B)A^-GluH \xrightarrow{k_{ET}} (Q_AQ_B^{-\bullet})A^-GluH \qquad (5b)$$

We indicate the individual rate constants of the underlying reaction scheme (eq 5a) by a nonitalic font, whereas the composite constants are in italics. The apparent second-order rate constant $k_{(2)}$ is a function of the binding of the acid (i.e., k_{on} and k_{off}) and the rate constant of proton transfer k_{H^+}, the value of which depends on the pK_a of the acid RH^+. The rate constant k_{H^+} is itself composed of individual rate constants k_1, k_{-1}, and k_2 as shown. The dashed lines (eq 5a) represent the reverse reactions that are slow compared to the forward steps (i.e., the rate of the reaction to continue in the forward direction exceeds that for it to return to the preceding state, e.g., $k_{off}' > k_{-2}$) and, therefore, do not contribute to the $k_{(2)}$ or k_{H^+}. We note that other intermediate states which have yet to be detected may exist within the pathway.

Table 1: Rate Constants Used for the Fit of the Brönsted Plot (Figure 6)[a]

rate constant	value	rate constant	value
$\mathbf{k_{on}}$	$\mathbf{1 \times 10^{10}\ M^{-1}\ s^{-1}}$	k_1^0	$10^{6\pm1}\ s^{-1}$
$\mathbf{k_{off}}$	$\mathbf{1 \times 10^{8}\ s^{-1}}$	k_{-1}^0	$10^{11\pm1}\ s^{-1}$
$\boldsymbol{k_{H^+}^0}$	$\mathbf{1 \times 10^{5}\ s^{-1}}$	k_2	$10^{10\pm1}\ s^{-1}$

[a] The three rate constants in the first column were determined from the fit of eqs 7 and 8 to the data in Figure 6. Their reliability is estimated to be within a factor of 2. The three rate constants in the third column were estimated by applying additional constraints (see text). They are reliable to an order of magnitude as indicated. The superscript 0 refers to rate constants for imidazole.

In the following sections, we discuss the individual steps involved in the chemical rescue. They provide the ingredients of a mathematical model that is fitted to the data to obtain the intrinsic equilibria and rate constants for proton transfer. From these results, we generate an energy landscape for the proton transfer process from the RC surface to the internal proton acceptor groups.

Binding of the Acid to the RC Surface. The first step in the chemical rescue of $k_{AB}^{(1)}$ (eq 5a) is the binding of the cationic rescuing acid RH^+ to the RC surface (eq 6).

$$RH^+ + A^-Glu^- \underset{k_{off}}{\overset{k_{on}}{\rightleftharpoons}} RH^+(A^-Glu^-) \qquad (6)$$

Quantitative values for the intrinsic rate constants were obtained from the measured values of the dissociation constant K_D and k_{on}. The linearity of the Brönsted plot over a large range of pK_a values (>7 pK_a units) of acids with differing structures suggests that there is no significant effect of the acid structure on K_D (i.e., k_{off}/k_{on}). Consequently, we assume that the K_D value of 10 mM determined for trimethylamine is the same for all acids used in this study.

The value of $k_{(2)}$ for low-pK_a acids provides an *estimate* for a diffusion-limited k_{on} of $\sim 10^{10}\ M^{-1}\ s^{-1}$ (Figure 6). Since $K_D = k_{off}/k_{on} = 10$ mM, the value of $k_{off} \cong 10^8\ s^{-1}$ (Table 1).

Steady State Approximation: Determination of the Proton Transfer Rate Constant. Since the rates of acid binding ($k_{on}[RH^+] \cong 10^6\ s^{-1}$ for $[RH^+] \cong 0.1$ mM) and leaving ($k_{off} \cong 10^8\ s^{-1}$) are much larger than the observed rate ($k_{AB}^{(1)} \cong 10^3\ s^{-1}$) [i.e., $k_{on}[RH^+]$, $k_{off} \gg k_{AB}^{(1)}$], the intermediate states reach a pseudo-steady state concentration during the observed reactions (*35*). We therefore apply a steady state approximation for the kinetic reaction scheme (eq 5a). The net rate constant $k_{(2)}$ is the product of the on-rate constant k_{on} and the probability that proton transfer proceeds to Glu-L212, given by the branching ratio of $k_{H^+}/(k_{off} + k_{H^+})$ (*35*). Thus, we express $k_{(2)}$ as

$$k_{(2)} = k_{on}\frac{k_{H^+}}{k_{off} + k_{H^+}} \qquad (7)$$

where k_{H^+} is the proton transfer rate constant for transfer from any of the rescuing bound acids to Glu-L212 (steps 2 and 3 in eq 5a). The pK_a dependence of k_{H^+} is due to transfer from RH^+ to A^- (step 2 in eq 5a) and can be expressed in terms of $k_{H^+}^0$, the rate constant for proton transfer from a surface-bound protonated His:

$$k_{H^+} = k^* \times 10^{-[pK_a(RH^+) - pK_a(AH)]} = k_{H^+}{}^0 \times 10^{-[pK_a(RH^+) - pK_a(His)]} \quad (8)$$

where k^* is the rate constant for isoenergetic proton transfer from RH^+ to A^- [i.e., $pK_a(RH^+) = pK_a(AH)$] and $pK_a(RH^+)$, $pK_a(AH)$, and $pK_a(His)$ are the pK_a values for RH^+, AH, and His, respectively. The determination of $k_{H^+}{}^0$ provides an estimate of the proton transfer rate constant in the native RC. Since the functional moeity of imidazole is analogous to that of the replaced imidazole groups of His-H126 and His-H128, we assume that imidazole is a good analogue of the surface-bound His and as a consequence $pK_a(His) \cong pK_a(imidazole)$.

We now use eqs 7 and 8 to fit the observed pK_a dependence of $k_{(2)}$ shown in Figure 6. Use of the additional constraint $K_D = k_{off}/k_{on} = 10$ mM reduces the number of free parameters for this fit to two. The resultant fitting parameters are shown in bold in Table 1. The value for $k_{H^+}{}^0$ was determined to be

$$k_{H^+}{}^0 \cong 10^5\ s^{-1} \quad (9)$$

with an uncertainty of a factor of approximately 2 (see Table 1). The good fit of the model to the observed pK_a dependence of $k_{(2)}$ (Figure 6) shows that this model adequately describes the behavior of all the acids used in this study and supports the initial assumption that the predominant kinetic difference between acids is the rate constant for proton transfer from RH^+ to A^-. In particular, any variation in K_D between acids over the measured range is minor compared to the magnitudes of the changes in the proton transfer rates. Our previous *estimates* for k_{on} and k_{off} (previous section) were within error the same as determined from the fit. Note that $k_{H^+}{}^0$ is larger than $k_{AB}{}^{(1)}$ by approximately 2 orders of magnitude (Figure 2), further justifying the use of a steady state approximation.

To gain a better qualitative understanding of the process, we shall now consider some limiting cases predicted by the model. One of the features of the model is the predicted change in the rate-controlling step for different acids. For acids with a $pK_a(RH^+)$ of <4, proton transfer from RH^+ to A^- (step 1 in eq 5a) is favorable. Therefore, a maximal rate of proton transfer is achieved, and the rate is limited by the rate of association at (diffusion to) the active site. Hence, $k_{(2)}$ reaches a maximum that is determined by the diffusion rate of the acid, which is *independent* of the acid pK_a. For acids with a $pK_a(RH^+)$ of >4, proton transfer from RH^+ to A^- is unfavorable. Thus, the rate of transfer is the product of the fraction of bound protonated acid (given by $1/K_D$, for our situation where $[RH^+] < K_D$) and the rate constant for proton transfer from RH^+ to A^- (k_{H^+}), which is strongly *dependent* on the pK_a of the acid. Thus, the rate law for the second-order rate constant $k_{(2)}$ is approximated by eq 10:

$$k_{(2)} \cong k_{on} \qquad pK_a(RH^+) < 4 \quad (10a)$$

$$k_{(2)} \cong \frac{k_{H^+}}{K_D} \qquad pK_a(RH^+) > 4 \quad (10b)$$

From a knowledge of $k_{(2)}$ and K_D, we obtain k_{H^+} using eq 10b.

A second method for estimating $k_{H^+}{}^0$ uses eq 8 and the limiting value measured for trimethylamine ($k_{H^+} \sim 130\ s^{-1}$). The proton transfer rate constant for transfer from imidazole ($k_{H^+}{}^0$) should be greater due to its 2.8 unit lower pK_a value (eq 8) by a factor of $10^{2.8}$, yielding a value of $\sim 10^5\ s^{-1}$ for $k_{H^+}{}^0$, the same as calculated above in eq 9. It should be noted that although $k_{H^+}{}^0$ was determined from the data acquired at pH 9, similar values of $k_{(2)}$ were obtained at pH 8.5 and 9.5, indicating that this rate constant is approximately pH independent. Thus, we suggest that $k_{H^+}{}^0$ is a good estimate at physiological pH values.

Proton Transfer to $Q_B^{-\bullet}$. In the above discussion, we determined the rate of proton transfer from the RC surface through the proton transfer pathway to Glu-L212 (Figure 1), which subsequently supplies this proton to Q_BH^- (*1*, *3*−*5*). The same approach was used to evaluate proton transfer to $Q_B^{-\bullet}$. A decrease in this rate was observed in the double-mutant RC (*24*). This proton transfer is coupled to electron transfer in an analogous manner, giving rise to an observed rate constant $k_{AB}{}^{(2)}$ ($Q_A^{-\bullet}Q_B^{-\bullet} + H^+ \rightleftarrows Q_A^{-\bullet}Q_BH^\bullet \rightarrow Q_AQ_BH^-$) that is rate-controlled by electron transfer in the native RC. In the double mutant RC, $k_{AB}{}^{(2)}$ was slower than in the native RC and became rate-controlled by proton transfer (*24*), which could similarly be increased by the addition of external cationic acids. However, the absolute values of $k_{AB}{}^{(2)}$ differ from those reported for $k_{AB}{}^{(1)}$. In particular, the limiting value measured with trimethylamine was ~5-fold smaller (data not shown). Although both $k_{AB}{}^{(2)}$ and $k_{AB}{}^{(1)}$ were enhanced, they did not reach the same values, indicating that internal proton transfer was rate-controlling. We estimate the rate constant of proton transfer associated with $k_{AB}{}^{(2)}$ from the surface-bound imidazole to $Q_B^{-\bullet}$ to be $\sim 2 \times 10^4\ s^{-1}$ by applying the second method for calculating $k_{H^+}{}^0$ described above. This value is consistent with previously proposed lower limits of $10^3\ s^{-1}$ for the proton transfer rate constant deduced from the observation that the rate constant of proton transfer is greater than $k_{AB}{}^{(2)}$ (*23*, *24*, *38*, *39*). The pathway for this proton transfer shares the involvement of the surface His-H126 and His-H128 (*24*), Asp-L210 and Asp-M17 (*23*), and Asp-L213 (*4*, *22*) (Figure 1). It differs at the internal terminus where Ser-L223 bridges the oxygen of Asp-L213 and the distal oxygen of Q_B (Figure 1). The smaller proton transfer rate constant may reflect the lower pK_a of $Q_BH^\bullet$ compared to that of Glu-L212 (i.e., $pK_a \sim 4.5$ vs 8.5) (*38*, *39*).

Importance of the Intermediate State for Fast Proton Transfer. The estimated rate constant of proton transfer in the bacterial RC over ~20 Å is comparable to that observed in carbonic anhydrase, in which proton transfer occurs over ~9 Å from the imidazole group of His-64 to a Zn^{2+}-OH^- (*28*, *30*). We attribute the fast rate over the larger distance reported here to the presence of the intermediate proton acceptor group A^-. If it is assumed that A^- is one or more of the electrostatically interacting carboxylic acids shown in Figure 1, each step in the proton transfer process occurs over ~9 Å (or less) bridged by water molecules. Thus, we postulate that the relatively fast rate of proton transfer over ~20 Å in the bacterial RC is achieved by breaking the proton transfer process into (at least) two sequential, shorter proton transfer steps.

Electrostatic Interaction between the Acid and the RC Surface: Determination of the pK_a of AH. Of fundamental

importance in determining the individual rate constants and the energy landscape for the stepwise proton transfer process is the determination of the pK_a of AH, which is related to $pK_a(RH^+)$ via the Brönsted plot (Figure 6). The decrease in $k_{(2)}$ with increasing salt concentrations (Figure 5) shows that there is an electrostatic attraction between the positively charged (protonated) acid and the negatively charged region of the RC surface at the entrance of the proton transfer pathway. This interaction energy increases the pK_a of the acid $pK_a(RH^+)$ upon binding. To determine the magnitude of the shift in $pK_a(RH^+)$ upon binding, we first evaluate the effective surface charge on the RC. From the Debye−Hückel limiting law, we relate the change in rate to the effective surface charges of the acid and the RC (eq 11) (*40*).

$$\log[k_{(2)}/k_{(2)}^*] = 2CZ_{RC}Z_{RH}[\Delta(I^{1/2})] \qquad (11)$$

where $k_{(2)}$ and $k_{(2)}^*$ are the second-order rate constants at two ionic strengths differing by ΔI, C is a constant [0.58 (25 °C) (*40*)], and Z_{RC} and Z_{RH} are the charges on the RC surface and the acid RH^+, respectively. Since $Z_{RH} = 1$ for the acid, Z_{RC} obtained from the slope of $\log[k_{(2)}]$ versus $\Delta I^{1/2}$ (Figure 5) is -1.8 ± 0.1. Thus, the second-order rate constant is electrostatically enhanced by the negative charge on the RC surface at the cytoplasmic entrance of the proton transfer pathway.

We estimate the interaction energy, $\delta\Delta G$ (in eV), using Coulomb's Law (eq 12).

$$\delta\Delta G = 14.4Z_{RC}Z_{RH}/\epsilon r \qquad (12)$$

where ϵ is the dielectric constant and r is the distance between two point charges (in Å) with magnitudes Z_{RC} and Z_{RH} (in electron charges). To estimate the distance r, we used the imidazole group of His-H126 in the native RC as a model for the bound imidazole (Figure 1). This results in an average distance of 6 Å between the imidazole proton and the oxygen atoms of the nearby carboxylic acids at the RC surface. A value of ~25 for ϵ was obtained from the empirical distance-dependent relation [$\epsilon = 1 + 60(1 - e^{-0.1R})$, where R is the distance between the two charges] (*41*). Using these values in eq 12, we obtain a rough estimate of the interaction energy $\delta\Delta G$ of $\sim 180 \pm 90$ meV. This interaction energy results in an increase in the pK_a of the acid upon binding of ~3 units,[6] which results in a pK_a of the bound imidazole of ~10. The increased pK_a deduced from this analysis is qualitatively consistent with elevated values of ~7−8 for the pK_a of His-H126 and/or His-H128 in the native RC which were determined from the pH dependence of metal binding (*42*, *43*) and the free energy for Q_B reduction (*44*). However, these experimental estimates of the pK_a of His are smaller than the value calculated above, suggesting that the energy of the interaction between the surface and the bound rescuing acid may be overestimated by ~2 pK_a units by using the empirical relation of the dielectric constant.

[6] The free energy difference between the proton donor (RH^+) and acceptor (A^-) [$\delta\Delta G = kT \ln K_{EQ}$ (k is Boltzmann's constant, and K_{EQ} is the equilibrium constant)] can be written in terms of δpK_a by noting that $\delta pK_a = -\log K_{EQ}$. Thus, $\delta\Delta G = -2.3kT\,\delta pK_a$. A pK_a change of 1 unit is equivalent to a change in $\delta\Delta G$ of ~60 meV at room temperature.

Having estimated the effect of binding on the pK_a of RH^+, we can now assess the pK_a of AH. As discussed above, the turning point in the Brönsted plot occurs approximately when $pK_a(RH^+) = pK_a(AH)$. For our situation with an intermediate acceptor group, a correction to the value of the pK_a from the value at the turning point is required,[5] yielding a solution pK_a of ~2 for RH^+. Once the RH^+ group binds to the RC surface, its pK_a is increased to between 3 and 5. Thus, $pK_a(AH)$ is between 3 and 5, suggesting that it is a carboxylic acid group.

The most likely candidates for the intermediate acceptor A^- are the carboxylates of Asp-L210, Asp-L213, Asp-M17, and Asp-H124, located between the imidazole binding site and the final proton acceptor groups in the RC interior (near the end of the red line in Figure 1). This group of acids forms an electrostatically interacting cluster (*8*, *9*) that may act as a single unit.

Individual Rate Constants and Energy Landscape for Proton Transfer from the Surface to Glu-L212. The energy landscape of the proton transfer process is determined by the individual rate constants that comprise k_{H^+}. To obtain their values, we first apply (in a manner analogous to eq 7) a steady state analysis to express $k_{H^+}{}^0$ as the product of $k_1{}^0$ and the branching ratio $k_2/(k_{-1}{}^0 + k_2)$ (see eq 5a):

$$k_{H^+}{}^0 = k_1{}^0 \frac{k_2}{k_{-1}{}^0 + k_2} \qquad (13)$$

where $k_1{}^0$ and $k_{-1}{}^0$ are the forward and reverse proton transfer rate constants, respectively, for transfer from imidazole to A^-. Since there are three unknown parameters ($k_1{}^0$, $k_{-1}{}^0$, and k_2) to fit one experimental number ($k_{H^+}{}^0$), we need additional constraints. The rate constant $k_1{}^0$ for proton transfer from bound imidazole to A^- can be no smaller than the overall proton transfer $k_{H^+}{}^0$ (10^5 s^{-1}) (eq 9); i.e., $k_1{}^0 \geq 10^5$ s^{-1}. An upper limit is established by noting that k_1 is not likely to be greater than 10^{12} s^{-1}, the rate of proton exchange in water or the first-order proton release from photoinduced superacids (*45*−*47*). This limit applies to bound acids with the greatest proton driving force, i.e., solution $pK_a \cong 2$. Thus, $k_1{}^0$ will be smaller due to the ~5 unit larger solution pK_a of imidazole; the same difference is obtained for the bound pK_a values since the electrostatic interaction with the surface is approximately the same for all buffers. Using eq 8, we estimate $k_1{}^0$ to be $\leq 10^7$ s^{-1} (i.e., 10^7 $s^{-1} \geq k_1{}^0 \geq 10^5$ s^{-1}). After binding has occurred, the pK_a of imidazole will increase by ~3 units (as discussed in a previous section) due to its electrostatic interaction with the charged RC surface. Thus, the ΔpK_a for proton transfer from the bound imidazole to AH is approximately −5. Therefore, $K_1{}^0 = k_1{}^0/k_{-1}{}^0 = 10^{-5}$, and 10^{12} $s^{-1} \geq k_{-1}{}^0 \geq 10^{10}$ s^{-1}. Using the Boltzmann factor and the range for $k_1{}^0$ in eq 13, k_2 is constrained to be between 10^9 and 10^{11} s^{-1}. The values of $k_1{}^0$, $k_{-1}{}^0$, and k_2 obtained from the constraints discussed above represent order of magnitude estimates. They are less well determined than the values of k_{on}, k_{off}, and k_{H^+} obtained from the fit to the Brönsted plot (see Table 1).

An approximate energy profile for the proton transfer process is obtained from the estimated values for the pK_as of the bound imidazole ($pK_a \cong 10$), AH ($pK_a \cong 5$), and Glu-L212 ($pK_a \cong 8.5$) (3−5).[3] Proton transfer from the bound

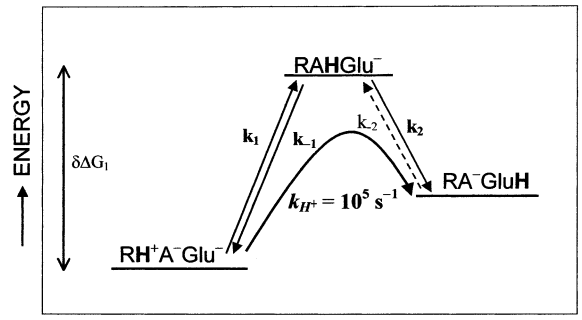

FIGURE 7: Energy level diagram of the states involved in the proton transfer reactions from the bound imidazole (RH^+) to Glu-L212, the final proton acceptor (eq 2). The rate constants are given in Table 1. Proton transfer proceeds through an intermediate state AH which is higher in energy than the initial state by ~300 meV ($\delta\Delta G_1$). Proton transfer can then proceed downhill by ~210 meV to Glu-L212. The resultant forward proton transfer rate k_{H^+} ($\cong 10^5$ s^{-1}) is shown. The reverse proton transfer (dashed arrow) contributes only at high rescuing acid concentrations.

protonated imidazole to A^- is unfavorable by ~300 meV (30 kJ/mol, 7 kcal/mol) due to the smaller pK_a of AH (~5 units). However, proton transfer from AH to Glu-L212 is favorable by ~210 meV due to the greater pK_a (~3.5 units) of Glu-L212. Thus, the uphill proton transfer to A^- is followed by a downhill proton transfer to Glu^- (Figure 7).

Although our experiments were performed on the bacterial RC, the approach described in this paper can be applied to other transmembrane systems, such as bacteriorhodopsin (*48*), cytochrome oxidase (*49*, *50*), and the cytochrome bc_1 complex (*51*, *52*), to evaluate the rates of proton transfer as well as the pK_as of the proton transfer components.

SUMMARY

The main goal of this study was to obtain the rate constant k_{H^+} for proton transfer through the physiological proton transfer pathway in the bacterial RC (eq 2), a bioenergetic system in which proton transfer is not rate-controlling for the electron transfer reactions. This was accomplished by the following strategy.

(1) Create an analogous system in which proton transfer becomes rate-controlling by removing surface amino acid side chains (proton donors) located at the entrance of the proton transfer pathways. The imidazole groups of the surface His-H126 and His-H128 were removed since (i) they were the most likely candidates of the proton transfer pathway that could be removed with little structural perturbations and (ii) their function could be restored by exogenous proton donors (rescuers) (RH^+) with essentially no structural constraints because the rescuing acid interacts with the protein surface.

(2) Determine conditions that provide the greatest difference in $k_{AB}^{(1)}$ between native and mutant RCs.

(3) Determine the effect of adding exogenous acids on $k_{AB}^{(1)}$ to obtain a second-order rate constant $k_{(2)}$ for the chemical rescue (eq 4). This was done over a wide range of concentrations and pK_a values. Rescue with acids having pK_a values at least 5 units smaller than imidazole was used to deduce the existence of an intermediate state (i.e., a change in the slope of the Brönsted plot).

(4) Measure the dissociation constants K_D of the acids (Figure 4).

(5) Develop a kinetic model (eq 5) to fit the observed pK_a dependence of $k_{(2)}$.

(6) Use the rate constants obtained from the fit to determine k_{H^+0} (eq 9). Upon application of additional constraints, an approximate energy profile for the proton transfer process could be deduced (Figure 7).

(7) Since the functional group of the bound imidazole rescuer is the same as that of His-H126 and His-H128 in the native RC, k_{H^+0} should be the same as in the native RC.

Thus, from the concentration dependence of the observed rate and the pK_a dependence of $k_{(2)}$ measured over a wide range, we were able to deduce the existence and pK_a value of an intermediate state, estimate its free energy, and determine the individual rate constants for proton transfer through a pathway that traverses ~20 Å.

Although the data presented in this paper apply to the bacterial RC, the general idea and strategy should be applicable to the study of long-distance proton transfer through other proteins.

ACKNOWLEDGMENT

We are grateful to Edward Abresch, Charlene Chang, Shannon Foster, and Jeanette Johnson for expert technical assistance and Herbert Axelrod, Rafael Calvo, Wolfgang Lubitz, and Charles Perrin for helpful discussions.

REFERENCES

1. Blankenship, R. E., Madigan, M. T., and Bauer, C. E. (1995) *Anoxygenic photosynthetic bacteria*, Kluwer Academic Publishers, Dordrecht, The Netherlands.
2. Okamura, M. Y., Paddock, M. L., Graige, M. S., and Feher, G. (2000) *Biochim. Biophys. Acta 1458*, 148−163.
3. Paddock, M. L., Rongey, S. H., Feher, G., and Okamura, M. Y. (1989) *Proc. Natl. Acad. Sci. U.S.A. 86*, 6602−6606.
4. Takahashi, E., and Wraight, C. A. (1992) *Biochemistry 31*, 855−866.
5. Ädelroth, P., Paddock, M. L., Sagle, L. B., Feher, G., and Okamura, M. Y. (2000) *Proc. Natl. Acad. Sci. U.S.A. 97*, 13086−13091.
6. Miksovska, J., Schiffer, M., Hanson, D. K., and Sebban, P. (1999) *Proc. Natl. Acad. Sci. U.S.A. 96*, 14348−14353.
7. Grafton, A. K., and Wheeler, R. A. (1999) *J. Phys. Chem. 103*, 5380−5387.
8. Alexov, E. G., and Gunner, M. R. (1999) *Biochemistry 38*, 8253−8270.
9. Lancaster, C. R. D., Michel, H., Honig, B., and Gunner, M. R. (1996) *Biophys. J. 70*, 2469−2492.
10. Nabedryk, E., Breton, J., Hienerwadel, R., Fogel, C., Mäntele, W., Paddock, M. L., and Okamura, M. Y. (1995) *Biochemistry 34*, 14722−14732.
11. Verméglio, A., and Clayton, R. K. (1977) *Biochim. Biophys. Acta 461*, 159−165.
12. Kleinfeld, D., Okamura, M. Y., and Feher, G. (1984) *Biochim. Biophys. Acta 766*, 126−140.
13. Sebban, P., Maróti, P., Schiffer, M., and Hanson, D. K. (1995) *Biochemistry 34*, 8390−8397.
14. Tiede, D. M., Vazquez, J., Cordova, J., and Marone, P. A. (1996) *Biochemistry 35*, 10763−10775.
15. Graige, M. S., Feher, G., and Okamura, M. Y. (1998) *Proc. Natl. Acad. Sci. U.S.A. 95*, 11679−11684.
16. Li, J., Gilroy, D., Tiede, D. M., and Gunner, M. R. (1998) *Biochemistry 37*, 2818−2829.
17. Ermler, U., Fritzsch, G., Buchanan, S. K., and Michel, H. (1994) *Structure 2*, 925−936.
18. Stowell, M. H., McPhillips, T. M., Rees, D. C., Soltis, S. M., Abresch, E., and Feher, G. (1997) *Science 276*, 812−816.
19. Abresch, E. C., Paddock, M. L., Stowell, M. H. B., McPhillips, T. M., Axelrod, H. L., Soltis, S. M., Rees, D. C., Okamura, M. Y., and Feher, G. (1998) *Photosynth. Res. 55*, 119−125.

20. Fritzsch, G., Kampmann, L., Kapaun, G., and Michel, H. (1998) *Photosynth. Res. 55*, 127−132.
21. Takahashi, E., and Wraight, C. A. (1990) *Biochim. Biophys. Acta 1020*, 107−112.
22. Paddock, M. L., Rongey, S. H., McPherson, P. H., Juth, A., Feher, G., and Okamura, M. Y. (1994) *Biochemistry 33*, 734−745.
23. Paddock, M. L., Ädelroth, P., Chang, C., Abresch, E. C., Feher, G., and Okamura, M. Y. (2001) *Biochemistry 40*, 6893−6902.
24. Ädelroth, P., Paddock, M. L., Tehrani, A., Beatty, J. T., Feher, G., and Okamura, M. Y. (2001) *Biochemistry 40*, 14538−14546.
25. Gerencser, L., Taly, A., Baciou, L., Maroti, P., and Sebban, P. (2002) *Biochemistry 41*, 9132−9138.
26. Toney, M. D., and Kirsch, J. F. (1989) *Science 243*, 1485−1488.
27. Huang, S., and Tu, S. C. (1997) *Biochemistry 36*, 14609−14615.
28. Earnhardt, J. N., Tu, C., and Silverman, D. N. (1999) *Can. J. Chem. 77*, 726−732.
29. Hays, A. M., Vassiliev, I. R., Golbeck, J. H., and Debus, R. J. (1999) *Biochemistry 38*, 11851−11865.
30. Silverman, D. N. (2000) *Biochim. Biophys. Acta 1458*, 88−103.
31. Zheng, R., and Blanchard, J. S. (2000) *Biochemistry 39*, 16244−16251.
32. Paddock, M. L., Adelroth, P., Beatty, J. T., Feher, G., and Okamura, M. Y. (2002) *Biophys. J. 82*, 517a−518a.
33. Keller, S., Beatty, J. T., Paddock, M. L., Breton, J., and Leibl, W. (2001) *Biochemistry 40*, 429−439.
34. Isaacson, R. A., Lendzian, E., Abresch, E. C., Lubitz, W., and Feher, G. (1995) *Biophys. J. 69*, 311−322.
35. Fersht, A. (1999) *Structure and Mechanism in Protein Science: A Guide to Enzyme Catalysis and Protein Folding*, W. H. Freeman and Co., New York.
36. Brönsted, J. N., and Pedersen, K. (1923) *Z. Phys. Chem. A 108*, 185.
37. Lowery, T. H., and Richardson, K. S. (1987) *Mechanism and Theory in Organic Chemistry*, Harper Collins Publishers, New York.
38. Graige, M. S., Paddock, M. L., Bruce, J. M., Feher, G., and Okamura, M. Y. (1996) *J. Am. Chem. Soc. 118*, 9005−9016.
39. Graige, M. S., Paddock, M. L., Feher, G., and Okamura, M. Y. (1999) *Biochemistry 38*, 11465−11473.
40. Connors, K. A. (1990) *Chemical Kinetics, The Study of Reaction Rates in Solution.* VCH Publishers, New York.
41. Warshel, A., Russell, S. T., and Churg, A. K. (1984) *Proc. Natl. Acad. Sci. U.S.A. 81*, 4785−4789.
42. Gerencser, L., Taly, A., Baciou, L., Maroti, P., and Sebban, P. (2002) *Biochemistry 41*, 9132−9138.
43. Sagle, L., Paddock, M. L., Feher, G., and Okamura, M. Y. (2002) *Biophys. J. 82*, 196a.
44. Ädelroth, P., Paddock, M. L., Beatty, J. T., Feher, G., and Okamura, M. Y. (2002) *Biophys. J. 82*, 197a.
45. Gutman, M., and Nachliel, E. (1990) *Biochim. Biophys. Acta 1015*, 391−414.
46. Brandsburg-Zabary, S., Fried, O., Marantz, Y., Nachliel, E., and Gutman, M. (2000) *Biochim. Biophys. Acta 1458*, 120−134.
47. Genosar, L., Cohen, B., and Huppert, D. (2000) *J. Phys. Chem. 104*, 6689−6698.
48. Lanyi, J. K. (1998) *J. Struct. Biol. 124*, 164−178.
49. Brzezinski, P., and Ädelroth, P. (1998) *J. Bioenerg. Biomembr. 30*, 99−107.
50. Mills, D. A., and Ferguson-Miller, S. (1998) *Biochim. Biophys. Acta 1365*, 46−52.
51. Zito, F., Finazzi, G., Joliot, P., and Wollman, F.-A. (1998) *Biochemistry 37*, 10395−10403.
52. Crofts, A. R., Hong, S., Ugulava, N., Barquera, B., Gennis, R., Guergova-Kuras, M., and Berry, E. A. (1999) *Proc. Natl. Acad. Sci. U.S.A. 96*, 10021−10026.

BI020419X